Research Article Vol. 57, No. 34 / 1 December 2018 / Applied Optics F15

applied optics

Near-diffraction-limited Bragg reflection waveguide lasers

Lijie Wang,[1,2] Zhen Li,[3] Cunzhu Tong,[1,*] Shili Shu,[1] Sicong Tian,[1] Jun Zhang,[1] Xin Zhang,[1] and Lijun Wang[1]

[1]State Key Laboratory of Luminescence and Applications, Changchun Institute of Optics, Fine Mechanics and Physics, Chinese Academy of Sciences, Changchun 130033, China
[2]Department of Electronic Materials Engineering, Research School of Physics and Engineering, the Australian National University, Canberra, ACT 2601, Australia
[3]School of Electronic Information Engineering, Changchun University of Science and Technology, Changchun 130022, China
*Corresponding author: tongcz@ciomp.ac.cn

Received 5 June 2018; revised 30 July 2018; accepted 30 July 2018; posted 31 July 2018 (Doc. ID 334374); published 27 August 2018

We report a near-diffraction-limited tapered Bragg reflection waveguide laser (BRL) with a 10 μm ridge width, which is significantly larger than the conventional design. The large mode expansion in the vertical waveguide enables a scalable increase in the ridge width for single lateral mode operation. The role of the taper angle in the performance of tapered BRLs with the intrinsic characteristics of a thick vertical waveguide was investigated. The results indicate that the BRL with a taper angle of 3° shows the best far-field performance. An extremely low vertical divergence angle of 14.5° and a lateral divergence as low as 2.8° for 95% power inclusion were realized. A continuous-wave power exceeding 1 W was demonstrated. Over the entire operating current range, the vertical beam is almost unchanged with an excellent beam quality (M^2) of about 1.3. Lateral beam width increases slightly at higher currents due to the increasing contribution of side lobes, but it still remains nearly diffraction-limited with a lateral M^2 of less than 2. Narrow beam divergence and high beam quality of the lasers allow simple and inexpensive collimation and coupling.

OCIS codes: (140.2020) Diode lasers; (140.3570) Lasers, single-mode; (140.3295) Laser beam characterization.

https://doi.org/10.1364/AO.57.000F15

1. INTRODUCTION

High power and high brightness diode lasers are promising for various applications such as fiber laser pumping, material processing, medical applications, and nonlinear frequency conversion [1]. The broad-area (BA) diode lasers are the most important type of diode lasers due to their ability of high output power and a simple manufacturing process. However, BA diode lasers usually suffer from large divergence and low beam quality, which is mainly dependent on the epitaxial layer design as well as the stripe geometry [2].

Conventional diode lasers usually have a large vertical far-field (FF) divergence of above 30° at the FWHM, making it difficult and expensive for beam collimation and coupling [3]. Some optimized epitaxial structures with enlarged spot size have reduced the vertical divergence angle down to below 20° (FWHM). These designs include the super-large optical cavity [4,5], double barrier separate confinement heterostructures [6], and inserting mode expansion layers [7–9]. However, these traditional total-internal-reflection (TIR) waveguides are limited by the onset of high-order transverse modes when reducing the divergence angle. Recently, a novel type of edge-emitting diode lasers based on a longitudinal photonic band crystal (LPBC) structure has been developed for reducing vertical divergence [10]. It can achieve a stable single transverse mode operation under super-large mode expansion because of the strong mode discrimination of photonic bandgap (PBG) guiding. LPBC lasers have demonstrated a narrow vertical divergence of below 10° at wavelengths ranging from 658 to 1060 nm [11–14]. However, the highly asymmetric near-field (NF) profile of the LPBC laser results in the vertical FF with some small side lobes and hence a larger vertical divergence over 20° for 95% power content [15]. In the other word, the LPBC lasers do not show good enough divergence angles in practical applications. To solve this problem, we succeeded in developing a modified Bragg reflection waveguide laser (BRL), which utilized dual-side periodical waveguides and a low index defect layer to effectively expand the vertical optical mode. As a result, a narrow vertical divergence of lower than 10° with 95% power inclusion had been demonstrated [16].

For some applications such as fiber coupling, the lateral beam quality of diode lasers is more important. The BRLs also suffer from the drawbacks of conventional BA lasers, i.e., poor

beam quality in the lateral direction because of the excitation of higher-order lateral modes [17]. A number of approaches, including tapered lasers [18], phase structures [19], mode filters [20], tilted cavity [21], plasmonic metasurfaces [22], and gain-tailored and current path structures [23,24], were utilized to control the optical mode behavior. Among these techniques, a tapered structure is the most promising way to achieve nearly diffraction-limited laser output, in which an index-guided ridge waveguide (RW) is used for mode filtering, and a tapered gain section is used as an amplifier. However, there were few investigations on the tapered lasers based on a Bragg reflection waveguide (BRW), where the thick top waveguide might give a totally different optimized condition on the lateral layout. In this paper, we present tapered BRLs with 10 μm wide RW in order to achieve ultra-low beam divergence in the lateral and vertical directions. Devices with different taper angles, $\alpha_{\mathrm{Tap}} = 3°, 4°, 5°$, are fabricated and studied. The results indicate that devices with a 3° taper angle offer the best performance. It delivers more than 1.0 W total output power under continuous wave (CW) operation while maintaining a good beam quality with M^2 of as low as 1.18 in the lateral direction. The vertical and lateral divergence angles remain to be lower than 15.2° and 4.1° (95% power included), respectively, in the whole operating range.

2. DEVICE DESIGN AND FABRICATION

A. Vertical Epitaxial Design

The BRL epitaxial structure mainly consists of a mode-localized defect layer sandwiched between *n*- and *p*-doped distributed Bragg reflectors (DBRs). The DBR is made up of periodically alternated low and high index materials with index values of n_L and n_H separately. The active region is located inside the defect layer. In the BRW, light is guided by the PBG effect instead of TIR in the vertical direction. Therefore, the guided mode can be confined in the core with an arbitrary effective index (n_{eff}) when the optical frequency lies in the PBG. Thus, there are two regimes of PBG guidance, i.e., $n_{\mathrm{eff}} < n_L$ and $n_L < n_{\mathrm{eff}} < n_H$. In the first, light propagates in all layers leading to an NF profile with periodically oscillated peaks separated by nulls, whose FF is double-lobed or multi-lobed [25]. While in the second regime ($n_L < n_{\mathrm{eff}} < n_H$), light propagates in the layers with a high index but is evanescent in the low-index layers, resulting in a Gaussian-shaped NF with small triangular oscillations, whose FF pattern will be single-lobed [16]. As single-lobed FF is more suitable for high-brightness applications, we will design the BRW structure operating in the second regimes.

Another major issue in designing is to ensure a large spot size of the fundamental mode and a strong discrimination of the high-order modes. By optimizing the layer thickness and composition of the defect layer, high and low index layers of the DBR, the fundamental mode size could expand appreciably to achieve extremely low vertical divergence. Furthermore, the BRW should be designed in such a way that only the fundamental mode is localized in the active region. All high-order modes are shifted away toward the substrate and *p*-contact layer, resulting in a much lower confinement factor than that of the fundamental mode. In order to reduce the free carrier absorption loss, a graded doping profile is generally employed with increasing doping concentration from the active region toward the substrate and *p*-contact layer. Adjustment of the composition and thickness of the cladding layer also permits us to enhance the leakage loss of high-order modes. Therefore, high-order modes suffer from a much lower modal gain and larger optical loss than the fundamental mode, resulting in a strong mode discrimination. This allows stable single-mode operation at a significant mode extension, resulting in an ultra-low vertical divergence.

In this work for lasers emitting around 808 nm, the active region consists of two 6 nm $GaAs_{0.86}P_{0.14}$ quantum wells (QWs) separated by a 10 nm $Al_{0.4}Ga_{0.6}As$ barrier and is embedded in the defect layers. The *p*-doped top and *n*-doped bottom DBR are composed of 10 periodically alternating pairs of $Al_{0.35}Ga_{0.65}As$ (100 nm) and $Al_{0.5}Ga_{0.5}As$ (600 nm) layers with graded interfaces. The defect layer utilizes 80 nm $Al_{0.4}Ga_{0.6}As$, which has a middle index between that of the high and low index layers in the DBR in order to suppress the local waveguiding effect of high index QWs. The doping concentration in the DBR is varied from 2×10^{16} cm^{-3} in the layer closest to the active region to 5×10^{18} cm^{-3} in the last layer, aiming at a low optical loss, while the electrical resistance remains acceptably low. The total epitaxial thickness of the designed BRL is about 16.5 μm.

Figure 1 shows its refractive index distribution and simulated optical field profiles of the fundamental mode and the first high-order mode. The calculated optical confinement factor of the fundamental mode is about 0.69%, which is 3.2 times larger than the first high-order mode. Furthermore, by employing a graded doping profile with increasing doping concentration from the active region to both sides, high-order modes having their maximum field intensity at a high doping area suffer from a larger absorption loss than the fundamental mode. According to the gain and loss discrimination, the BRL can operate on a stable single transverse mode. From our calculations, the broad expansion of the fundamental mode gives rise to a narrow vertical beam divergence of about 6.5° (FWHM).

B. Lateral Structure Design

The scheme of the tapered BRL is shown in Fig. 2. It consists of an index-guided straight RW section followed by a gain-guided tapered section. The straight RW section serves as a modal

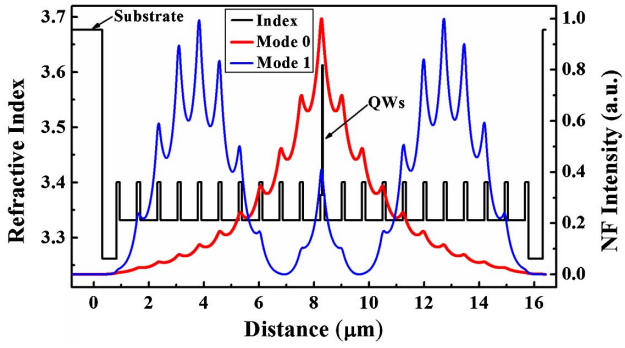

Fig. 1. Refractive index profile (black line) and calculated near-field amplitude of the fundamental mode (red line) and first high-order mode (blue line) for the BRL.

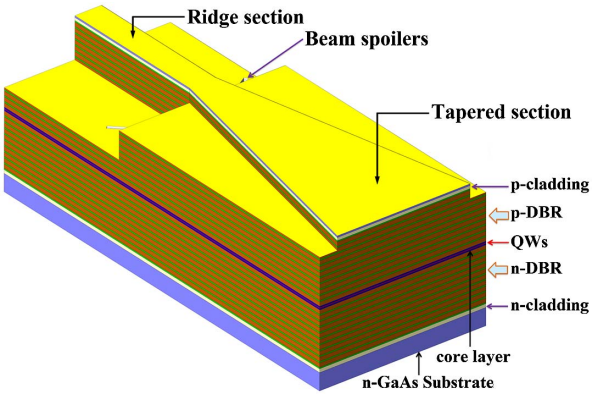

Fig. 2. Diagram of the tapered BRL.

filter, emitting a single spatial mode into the tapered section, where the laser is amplified while keeping nearly diffraction limited. The geometric parameters of the cavity play a significant role in determining the device performance [26].

The width and etching depth of the RW determine the mode size and free diffraction angle of the beam injected into the tapered section. Wider RW can improve the threshold gain and slope efficiency due to the reduced propagation loss and better heat dissipation, which also results in a small lateral diffraction angle. However, the RW width should not exceed the cutoff condition of high-order lateral modes, avoiding the multimode operation and consequent poor beam quality. Therefore, the optimal value of the RW width lies between the single-mode and double-mode operation regimes. The length of the straight ridge also has a strong impact on the beam quality. Short RW has a poor filtering effect of the higher-order modes, leading to rapidly deteriorated beam quality at high power operation. Generally, the RW length should be larger than 500 μm [27].

The optimization of the taper angle is a key point to improve the performance of tapered lasers, which should be close to the free diffraction angle of RW [28]. For small taper angles (narrower than the lateral diffraction limit), the beam follows the taper shape, yielding high beam quality but low output power due to high power density in the cavity. If the taper angle exceeds the free diffraction angle of RW, the large mode expansion admits higher output powers but at the cost of beam quality degradation. The wider angle causes a mismatch between the fundamental optical mode and the current injection profile. The excessive gain at the edges of the tapered section leads to the excitation of higher-order lateral modes and side lobes in the optical field.

For a fixed taper angle, stretching the length of the tapered section is advantageous for higher output power due to a wider output facet, with the lateral beam quality nearly undegenerated [29]. However, there exists a trade-off value for the taper lengths between high output power and high conversation efficiency related to the internal loss. Cavity-spoiling grooves at the sides of the RW section can be etched down through the active region for sufficient suppressing of the radiation reflected back. Antireflection-coated facets also enable improved spatial mode filtering and beam quality.

The epitaxial design also has a large impact on the lateral beam quality due to the interaction of the lateral and vertical optical field [30]. Except for the indirect (threshold, efficiency, power) influences, the epitaxial design has an important impact on the temperature profile in the vertical and lateral directions. It determines the bowing of the thermal lens, which influences the lateral beam quality and hence maximum achievable brilliance. In addition, the epitaxial layer structure with low optical confinement factor can reduce the dependence of index variation on the carrier density, leading to a weak tendency to filamentation [31]. Last, the current injection profile and lateral current spreading of lasers depend on the details of the epitaxial layers. The lateral carrier accumulation at the stripe edge may give excessive gain to high-order modes and lead to beam quality degradation. Based on the above effects, it opens a possibility to increase the lateral beam quality by proper design of the epitaxial structure.

In this work, the RW section length was chosen to be 750 μm for effective mode filtering. In order to support only the fundamental mode, the RW width and etching depth were optimized depending on the vertical layer structure. For the BRL studied in this paper, the thick BRW in the vertical direction leads to weaker interaction of the optical field with the ridge edges and the active area, which could suppress higher-order lateral mode lasing and reduce the generation of beam filamentation. Therefore, single lateral mode operation can be achieved for the case of a stripe width approximately equal to the vertical waveguide thickness [5]. Therefore, we utilized a large RW width of 10 μm in the tapered BRL, which is helpful to expand the optical mode size and reduce the lateral divergence. We have experimentally fabricated 10 μm wide ridge BRL and obtained nearly diffraction-limited beam output with the lateral divergence angle of 9.8°–11° (95% power content) at different currents. The corresponding diffraction angle in the tapered section is 2.8°–3.3° (95% power content), which is similar with the simulation result by a 2D effective index model. The taper length was kept constant at 1.5 mm, but the full taper angle was varied at 3°, 4°, and 5° to investigate its influence on the device performance. The corresponding output facet widths were 89, 115, and 141 μm, respectively. To enhance the mode filtering, a pair of cavity-spoiling grooves were introduced symmetrically on both sides of the RW.

C. Device Fabrication

The laser structure was grown by metal-organic vapor phase epitaxy. After the growth, the lateral structure of the tapered BRLs was fabricated as follows. First, the mesas of the RW section and the tapered section were etched simultaneously with a depth of 1.5 μm by inductive coupled plasma (ICP) etching. The RW mesa was further etched with a depth of 4 μm, while the tapered section was protected by photoresist. Then, the cavity-spoiling grooves were etched down to the active region by ICP etching. A 200 nm SiO_2 electrical insulating layer was deposited by plasma-enhanced chemical vapor deposition, and a contact window opening was created by reactive ion etching (RIE), followed by the standard *p*-side metal contact deposition. After the substrate thinning and *n*-side metallization, the diode lasers were cleaved into single devices without any passivation or coating. Finally, the devices were mounted

junction-side down on C-mount copper heatsinks using indium solder.

3. RESULTS

Figure 3 shows the light–current curves of the fabricated tapered BRLs with 3°, 4°, and 5° taper angles under CW operation. As can be seen, the device with 3° taper angle depicts the lowest threshold current of 0.46 A, and the maximum total power exceeds 1.1 W, limited by the thermal rollover. A higher power of 1.25 W is attainable for wider angle devices with a 4° taper angle. However, the laser with $\alpha_{\mathrm{Tap}} = 5°$ reveals the highest threshold current of 1.23 A and the lowest output power of only 0.9 W, which is seriously limited by the thermal load due to the large threshold current.

The threshold current density was 563 A/cm^2, 701 A/cm^2, and 994 A/cm^2, respectively, for the 3°, 4°, and 5° tapered lasers. The increase of threshold current density may be simply a consequence of higher optical losses. As in our fabricated devices, the free diffraction angle of RW in the cavity is about 3° (95% power content). For the device with 4° and 5° taper angles, the laser beam leaving the RW section cannot fully cover the tapered section. The poor coverage between the gain area and light field results in a higher cavity loss. The lasing spectrum of the lasers with 3° taper angle is shown in the inset of Fig. 3, which is measured by an AQ6370C optical spectrum analyzer at 1.0 A current. As can be seen, the spectrum shows a narrowband emission with a peak wavelength of 808.35 nm and a spectral width (FWHM) of about 0.05 nm.

Figure 4 shows the measured vertical FF distributions of the device with a 3° taper angle at various operating currents. The FWHM-defined vertical divergence angle is determined to be 6.5°–6.9°, which is stable with increasing currents. The envelope of its intensity profile is close to a Gaussian distribution. The vertical divergence for 95% power inclusion is lower than 15.2° over the full range, being considerably narrower than that of conventional diode lasers. The nearly identical characteristics of vertical FF divergence are obtained in the devices with 4° and 5° taper angles.

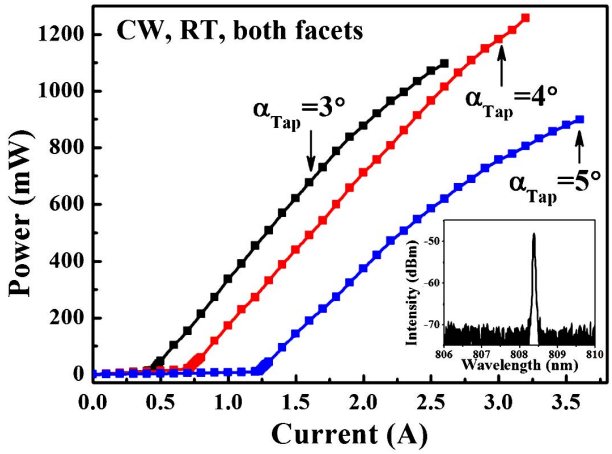

Fig. 3. Experimental light–current characteristics as a function of taper angle. Inset shows the spectrum of lasers with $\alpha_{\mathrm{TAP}} = 3°$ at 1.0 A current.

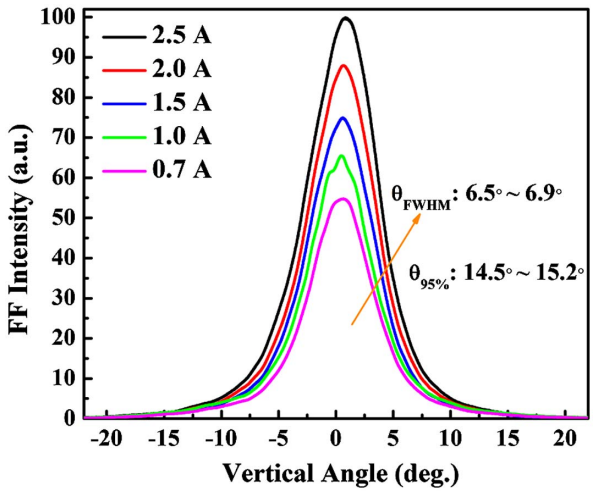

Fig. 4. Measured vertical FF profiles of laser with $\alpha_{\mathrm{TAP}} = 3°$ at different currents.

Figure 5 shows the influence of current on the lateral FF profiles for the devices with taper angles of 3°, 4°, and 5°, respectively. For the device with a taper angle of 3°, the lateral divergence is 1.7° (FWHM) and 3.8° (95% power inclusion) at 0.7 A. It reduces to 1.0° (FWHM) and 2.8° (95% power

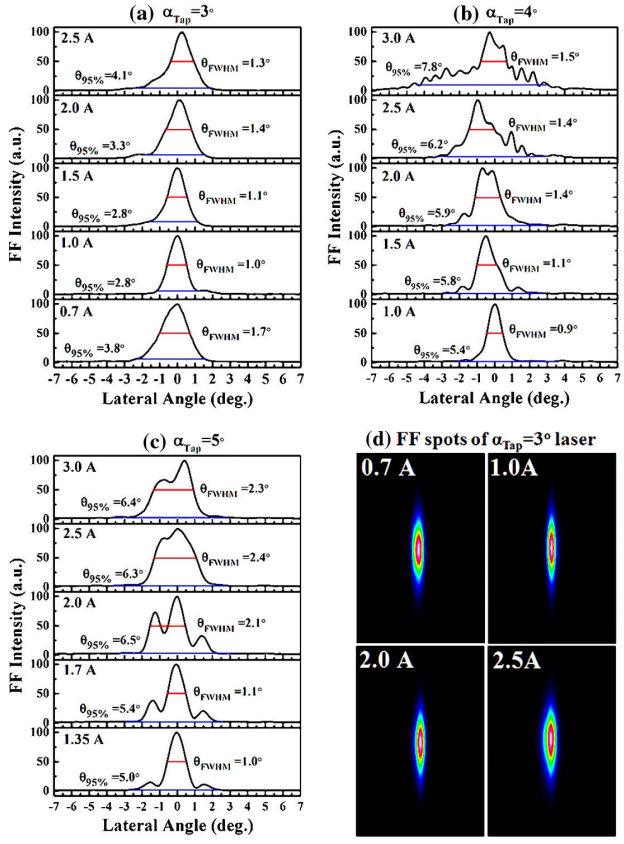

Fig. 5. Measured lateral FF distributions of devices with (a) $\alpha_{\mathrm{Tap}} = 3°$, (b) $\alpha_{\mathrm{Tap}} = 4°$, and (c) $\alpha_{\mathrm{Tap}} = 5°$ as a function of injected current. (d) Measured FF patterns of the tapered BRL with $\alpha_{\mathrm{Tap}} = 3°$ under CW operation at various currents.

inclusion) at 1.0 A. The narrowed FF with increasing current can be attributed to the enlarged waist beam size under high bias current. When the current is increased further, the lateral divergence slightly increases. At currents above 2.0 A, a weak side lobe occurs, and the power in the central lobe decreases, leading to a broadened lateral FF. However, the relative position and power of the central lobe only changes slightly. In contrast, the devices with angles of 4° and 5° show much worse FF. As seen in Fig. 5(b), the FF profile of the device with 4° taper angle shows a clearly pronounced main lobe in the center at low current. When the current is above 1.5 A, many obvious side peaks begin to appear. Although its lateral FF width at the FWHM level remains at a constant value, the side lobes beyond the central lobe result in a much larger divergence angle of 5.4°–7.8° defined by 95% power content. In addition, the relative position and intensity of side peaks change significantly. On the other hand, the wider device with $\alpha_{\mathrm{Tap}} = 5°$ seen in Fig. 5(c) shows a wide envelope in the FF at high currents.

The lasers with various taper angles all suffer from a widening lateral FF at high injection current, a so-called FF blooming effect. The predominant cause for the FF blooming is current-induced heating and the resulting thermal lensing phenomenon [32]. Under high power operation, the increasing heating enhances the lateral thermal gradient, inducing a larger lateral index step between the center and its surrounding. This results in tighter confinement of the fundamental mode as well as the onset of higher-order modes, broadening the lateral FF. Furthermore, for the devices with 4° and 5° taper angles, which are larger than the free diffraction angle of RW, the mismatch between the fundamental optical mode and the injection current profile leads to excessive gain at the edges of the tapered section [33]. In this case, high-order modes with a wide optical field are easy to be excited. In addition, the side lobes near the device edges grow appreciably during the backward propagation due to the higher gain, deteriorating the FF patterns.

At 3 A current, the FF profile of the device with 4° taper angle suffers from a progressive increase of side lobes beside the central lobe. The appearance of multiple peaks is mainly attributed to the onset of the filamentation, which causes high spatial frequency modulation in the NF distribution. The filamentation and resulting NF modulation depth are related to the material gain and power density (carrier density). Therefore, one effective way to suppress the filamentation is to reduce the power density by increasing the spreading of the optical energy. For the device with 5° taper angle, the wide output facet results in a lower power density than that of the device with 4° taper angle, delaying the occurrence of filamentation to higher power levels. For the device with a small taper angle (3°), the filamentation can be suppressed effectively due to the effective mode filtering and a better matching of the photons and carriers [34]. Therefore, the FF profile with multiple peaks does not appear in the devices with 3° and 5° taper angles.

Comparing the lateral FF profiles, only the device with 3° taper angle remains relative low divergence even under high injection conditions. The corresponding FF patterns were measured and are shown in Fig. 5(d). As it shows, the laser outputs a single-lobed and nearly diffraction-limited beam. The beam shape and width in the vertical direction are almost independent of the current, indicating a stable single transverse mode operation. In the lateral direction, the beam width first reduces and then slightly increases with increasing current, while the beam shape is only changed slightly. This demonstrates that the RW section and groove could effectively filter the high-order modes generated in the tapered section.

The beam quality M^2 of the tapered BRL with 3° taper angle was measured by a commercial beam propagation analyzer M2MS-BP209 according to the ISO11146 standard. During the measurement, the output light was first collimated by a commercial spherical lens and then focused into an artificial beam waist. Typical fast- and slow-axis respective collimation for traditional diode lasers was not employed. The beam width surrounding the beam waist is measured by a detector at a series of positions along the beam axis. M^2 is calculated from the measured beam width versus distance plot by a hyperbolic fitting. In the tapered lasers, the light diverges in the lateral direction from a virtual source inside the device, while the beam emits from the output facet in the vertical direction. Because of the large astigmatism of tapered lasers and our simple collimation optics, we measured the vertical and lateral M^2 values, respectively.

M^2 in the vertical direction remains about 1.3 across the whole operating current range, implying a stable vertical mode operation. The measured lateral M^2 parameters plotted in Fig. 6 show the lowest value of 1.18 at 1.0 A, which demonstrates a nearly diffraction-limited beam. The slight increase of the lateral M^2 at high injection currents mainly resulted from the growing contribution of side lobes, which results in larger deviations of the laser beams from an ideal Gaussian shape at higher output powers. However, the lateral M^2 remains well below 2, indicating excellent beam quality and high brightness of the tapered BRL. It demonstrates that the tapered BRL with a large RW width is advantageous for achieving low beam divergence while maintaining high beam quality.

A good BRL should have higher output power, better beam quality, and lower beam divergence, which are attractive

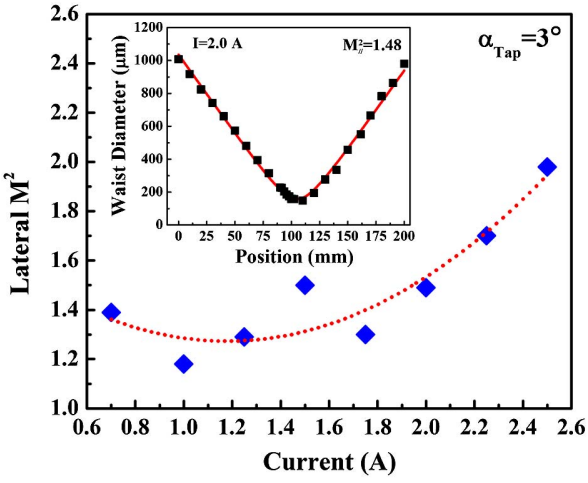

Fig. 6. Lateral M^2 of the tapered BRL with $\alpha_{\mathrm{Tap}} = 3°$ at different currents under CW operation. Inset shows the beam width in lateral direction along the beam axis at 2.0 A.

qualities in high brightness laser applications. However, the fabricated tapered lasers suffer from a widening lateral FF and increasing M^2 value with increasing current. Thermal lensing effect, excess carrier accumulation at the device edges, and filamentation are the most critical factors responsible for the beam quality degradation at high injection current. Furthermore, the astigmatism of the tapered laser is large and varied with the operation current, making the beam collimation difficult for fiber coupling. Therefore, the devices need further improvement to achieve high brightness and stable beam output, which are beneficial in practical applications due to large robustness against the variations of operating condition.

4. CONCLUSIONS

In summary, we have demonstrated a high-brightness BRL based on a tapered waveguide with relatively large RW width. The influence of taper angle on the beam properties was investigated in detail. It was shown that the tapered BRL with a taper angle of 3° had superior beam quality for a wider range of operating conditions. The vertical and lateral divergence angles are as low as 6.5° and 1.0° (FWHM) or 14.5° and 2.8° (95% power inclusion), respectively, which are much narrower than that of conventional lasers, including those with tapered structures. This nearly diffraction-limited BRL could satisfy the demand of external beam-shaping optics in applications such as high-efficiency fiber coupling. We believe these results will contribute to the development of high-brightness diode lasers.

Funding. National Natural Science Foundation of China (NSFC) (61474119, 61761136009, 61774153, 61774156); External Cooperation Program of Chinese Academy of Sciences (CAS) (181722KYSB20160005); Natural Science Foundation of Jilin Province (20160101243JC, 20180519024JH); China Scholarship Council (CSC) (201704910183).

Acknowledgment. The authors would like to thank Hui Li from Qingdao University of Science and Technology for fruitful discussions and paper editing.

REFERENCES

1. K. Paschke, F. Bugge, G. Blume, D. Feise, and G. Erbert, "High-power diode lasers at 1178 nm with high beam quality and narrow spectra," Opt. Lett. **40**, 100–102 (2015).
2. M. M. Karow, C. Frevert, R. Platz, S. Knigge, A. Maaßdorf, G. Erbert, and P. Crump, "Efficient 600-W-laser bars for long-pulse pump applications at 940 and 975 nm," IEEE Photon. Technol. Lett. **29**, 1683–1686 (2017).
3. B. Corbett, P. Lambkin, J. O'Callaghan, S. Deubert, W. Kaiser, J. P. Reithmaier, and A. Forchel, "Modal analysis of large spot size, low output beam divergence quantum-dot lasers," IEEE Photon. Technol. Lett. **19**, 916–918 (2007).
4. A. Pietrzak, H. Wenzel, G. Erbert, and G. Trankle, "High-power laser diodes emitting light above 1100 nm with a small vertical divergence angle of 13°," Opt. Lett. **33**, 2188–2190 (2008).
5. A. Pietrzak, H. Wenzel, P. Crump, F. Bugge, J. Fricke, M. Spreemann, G. Erbert, and G. Tränkle, "1060-nm ridge waveguide lasers based on extremely wide waveguides for 1.3-W continuous-wave emission into a single mode with FWHM divergence angle of 9° × 6°," IEEE J. Quantum Electron. **48**, 568–575 (2012).
6. C. T. Hung and T. C. Lu, "830-nm AlGaAs-InGaAs graded index double barrier separate confinement heterostructures laser diodes with improved temperature and divergence characteristics," IEEE J. Quantum Electron. **49**, 127–132 (2013).
7. B. Qiu, H. M. Hu, W. Wang, J. Ho, W. Liu, L. Kuang, T. Wang, and S. Wu, "830-nm InGaAs quantum well lasers with very low beam divergence," IEEE Photon. J. **9**, 2500308 (2017).
8. G. W. Yang, G. M. Smith, M. K. Davis, A. Kussmaul, D. A. S. Loeber, M. H. Hu, H. K. Nguyen, C. E. Zah, and R. Bhat, "High-performance 980-nm ridge waveguide lasers with a nearly circular beam," IEEE Photon. Technol. Lett. **16**, 981–983 (2004).
9. V. Shchukin, N. Ledentsov, K. Posilovic, V. Kalosha, T. Kettler, D. Seidlitz, M. Winterfeldt, D. Bimberg, N. Yu Gordeev, L. Ya Karachinsky, I. I. Novikov, Y. M. Shernyakov, A. V. Chunareva, M. V. Maximov, F. Bugge, and M. Weyers, "Tilted wave lasers: a way to high brightness sources of light," IEEE J. Quantum Electron. **47**, 1014–1027 (2011).
10. N. N. Ledentsov and V. A. Shchukin, "Novel concepts for injection lasers," Opt. Eng. **41**, 3193–3204 (2002).
11. M. V. Maximov, Y. M. Shernyakov, I. I. Novikov, L. Y. Karachinsky, N. Yu. Gordeev, U. Ben-Ami, D. Bortman-Arbiv, A. Sharon, V. A. Shchukin, N. N. Ledentsov, T. Kettler, K. Posilovic, and D. Bimberg, "High-power low-beam divergence edge emitting semiconductor lasers with 1- and 2-D photonic bandgap crystal waveguide," IEEE J. Sel. Top. Quantum Electron. **14**, 1113–1122 (2008).
12. M. J. Miah, T. Kettler, K. Posilovic, V. P. Kalosha, D. Skoczowsky, R. Rosales, D. Bimberg, J. Pohl, and M. Weyers, "1.9 W continuous-wave single transverse mode emission from 1060 nm edge-emitting lasers with vertically extended lasing area," Appl. Phys. Lett. **105**, 151105 (2014).
13. L. Liu, H. Qu, Y. Liu, Y. Zhang, Y. Wang, A. Qi, and W. Zheng, "High-power narrow-vertical-divergence photonic band crystal laser diodes with optimized epitaxial structure," Appl. Phys. Lett. **105**, 231110 (2014).
14. Md. J. Miah, V. P. Kalosha, D. Bimberg, J. Pohl, and M. Weyers, "Astigmatism-free high-brightness 1060 nm edge-emitting lasers with narrow circular beam profile," Opt. Express **24**, 30514–30522 (2016).
15. L. Liu, H. Qu, Y. Liu, Y. Wang, A. Qi, X. Guo, P. Zhao, Y. Zhang, and W. Zheng, "Design and analysis of laser diodes based on the longitudinal photonic band crystal concept for high power and narrow vertical divergence," IEEE J. Sel. Top. Quantum Electron. **21**, 1900107 (2015).
16. L. Wang, C. Tong, S. Tian, S. Shu, Y. Zeng, J. Rong, H. Wu, E. Xing, Y. Ning, and L. Wang, "High-power ultralow divergence edge-emitting diode laser with circular beam," IEEE J. Sel. Top. Quantum Electron. **21**, 1501609 (2015).
17. M. Winterfeldt, P. Crump, H. Wenzel, G. Erbert, and G. Tränkle, "Experimental investigation of factors limiting slow axis beam quality in 9xx nm high power broad area diode lasers," J. Appl. Phys. **116**, 063103 (2014).
18. A. Müller, C. Zink, J. Fricke, F. Bugge, O. Brox, G. Erbert, and B. Sumpf, "1030 nm DBR tapered diode laser with up to 16 W of optical output power," Proc. SPIE **10123**, 101231B (2017).
19. H. C. Eckstein, U. D. Zeitner, A. Tünnermann, W. Schmid, U. Strauss, and C. Lauer, "Mode shaping in semiconductor broad area lasers by monolithically integrated phase structures," Opt. Lett. **38**, 4480–4482 (2013).
20. J. Rong, E. Xing, Y. Zhang, L. Wang, S. Shu, S. Tian, C. Tong, X. Chai, Y. Xu, H. Ni, Z. Niu, and L. Wang, "Low lateral divergence 2 μm InGaSb/AlGaAsSb broad-area quantum well lasers," Opt. Express **24**, 7246–7252 (2016).
21. D. Heydari, Y. Bai, N. Bandyopadhyay, S. Slivken, and M. Razeghi, "High brightness angled cavity quantum cascade lasers," Appl. Phys. Lett. **106**, 091105 (2015).
22. M. Papaioannou, E. Plum, J. Valente, E. T. F. Rogers, and N. I. Zheludev, "Two-dimensional control of light with light on metasurfaces," Light Sci. Appl. **5**, e16070 (2016).
23. T. Wang, C. Tong, L. Wang, Y. Zeng, S. Tian, S. Shu, J. Zhang, and L. Wang, "Injection insensitive lateral divergence in broad-area diode lasers achieved by spatial current modulation," Appl. Phys. Express **9**, 112102 (2016).

24. M. Winterfeldt, P. Crump, S. Knigge, A. Maaßdorf, U. Zeimer, and G. Erbert, "High beam quality in broad area lasers via suppression of lateral carrier accumulation," IEEE Photon. Technol. Lett. **27**, 1809–1812 (2015).
25. L. Wang, C. Tong, Y. Zeng, Y. Yang, H. Peng, S. Tian, H. Wu, and L. Wang, "Bragg reflection waveguide twin-beam laser," Laser Phys. **23**, 105802 (2013).
26. L. Borruel, H. Odriozola, J. M. G. Tijero, I. Esquivias, S. Sujecki, and E. C. Larkins, "Design strategies to increase the brightness of gain guided tapered lasers," Opt. Quantum Electron. **40**, 175–189 (2008).
27. B. Sumpf, R. Hülsewede, G. Erbert, C. Dzionk, J. Fricke, A. Knauer, W. Pittroff, P. Ressel, J. Sebastian, and G. Tränkle, "High brightness 735 nm tapered lasers–optimisation of the laser geometry," Opt. Quantum Electron. **35**, 521–532 (2003).
28. J. M. G. Tijero, L. Borruel, M. Vilera, A. Perez-Serrano, and I. Esquivias, "Analysis of the performance of tapered semiconductor optical amplifiers: role of the taper angle," Opt. Quantum Electron. **47**, 1437–1442 (2015).
29. J. M. G. Tijero, L. Borruel, M. Vilera, A. Consoli, and I. Esquivias, "Simulation and geometrical design of multi-section tapered semiconductor optical amplifiers at 1.57 μm," Proc. SPIE **9134**, 91342A (2014).
30. M. Winterfeldt, J. Rieprich, S. Knigge, A. Maaßdorf, M. Hempel, R. Kernke, J. W. Tomm, G. Erbert, and P. Crump, "Assessing the influence of the vertical epitaxial layer design on the lateral beam quality of high-power broad area diode lasers," Proc. SPIE **9733**, 97330O (2016).
31. G. C. Dente, "Low confinement factors for suppressed filaments in semiconductor lasers," IEEE J. Quantum Electron. **37**, 1650–1653 (2001).
32. J. Rieprich, M. Winterfeldt, J. Tomm, R. Kernke, and P. Crump, "Assessment of factors regulating the thermal lens profile and lateral brightness in high power diode lasers," Proc. SPIE **10085**, 1008502 (2017).
33. S. Newton, K. Nyirenda, S. Bull, J. J. Lim, K. Hasler, J. Fricke, and E. C. Larkins, "Factors influencing brightness and beam quality of conventional and distributed Bragg reflector tapered laser diodes in absence of self-heating," IET Optoelectron. **8**, 99–107 (2014).
34. E. Pnie, B. Dalin, S. Golod, S. Goldin, and E. Sheke, "Types of filamentation in tapered diode amplifiers: their causes and features," Opt. Quantum Electron. **47**, 1535–1544 (2015).